


ARTICLE



Ubiquitin ligase E3 HUWE1/MULE targets transferrin receptor for degradation and suppresses ferroptosis in acute liver injury

Yan Wu^{1,6}, Huike Jiao^{1,6}, Yangbo Yue^{1,6} , Kang He^{2,6} , Yuting Jin², Jiang Zhang², Jing Zhang¹, Yuehan Wei³, Hanyan Luo¹, Zhenyue Hao⁴, Xuyun Zhao⁵, Qiang Xia^{1,6} , Qing Zhong^{1,6}  and Jing Zhang¹ 

© The Author(s), under exclusive licence to ADMC Associazione Differenziamento e Morte Cellulare 2022

Hepatic ischemia followed by reperfusion (I/R), a major clinical problem during liver surgical procedures, can induce liver injury with severe cell death including ferroptosis which is characterized by iron-dependent accumulation of lipid peroxidation. The HECT domain-containing ubiquitin E3 ligase HUWE1 (also known as MULE) was initially shown to promote apoptosis. However, our preliminary study demonstrates that high expression of HUWE1 in the liver donors correlates with less injury and better hepatic function after liver transplantation in patients. Thus, we investigate the role of HUWE1 in acute liver injury, and identify HUWE1 as a negative ferroptosis modulator through transferrin receptor 1 (TfR1). Deficiency of Huwe1 in mice hepatocytes (HKO) exacerbated I/R and CCl₄-induced liver injury with more ferroptosis occurrence. Moreover, suppression of Huwe1 remarkably enhances cellular sensitivity to ferroptosis in primary hepatocytes and mouse embryonic fibroblasts. Mechanistically, HUWE1 specifically targets TfR1 for ubiquitination and proteasomal degradation, thereby regulates iron metabolism. Importantly, chemical and genetic inhibition of TfR1 dramatically diminishes the ferroptotic cell death in *Huwe1* KO cells and *Huwe1* HKO mice. Therefore, HUWE1 is a potential protective factor to antagonize both aberrant iron accumulation and ferroptosis thereby mitigating acute liver injury. These findings may provide clinical implications for patients with the high-expression *Huwe1* alleles.

Cell Death & Differentiation (2022) 29:1705–1718; <https://doi.org/10.1038/s41418-022-00957-6>

INTRODUCTION

Liver injury and hepatic cell death are common features of all liver diseases. Liver transplantation is an established lifesaving treatment for end-stage liver disease. However, warm ischemia/reperfusion (I/R) injury represents one of the most challenging problems due to the technical feature of organ transplantation [1, 2]. Thus, it's of great significance to understand the pathogenesis of acute liver injury such as I/R in liver transplantation. Cell death in the liver is mainly executed by apoptosis or necrosis [3]. In recent years, several distinct forms of programmed cell death (PCD) have been defined with unique cellular mechanisms, among which an increasing level of interest has been manifested with regard to ferroptosis, a non-apoptotic form of regulated cell death [4]. Ferroptosis is induced by excess accumulation of phospholipid hydroperoxides, generated through oxidation of the polyunsaturated fatty acyl (PUFA) moieties of membrane phospholipids and catalyzed by iron-dependent mechanisms [5, 6]. As a pathological cell death, ferroptosis has been attributed to various oxidative stress-related diseases, including ischemia/reperfusion injury and neurodegenerative diseases [7–9].

As is evident from the name itself, accumulated intracellular iron is one of the key factors for the execution of ferroptosis. Excess iron, both ferrous ion Fe²⁺ and ferric ion Fe³⁺, react with

hydrogen peroxide (H₂O₂) to yield hydroxyl and hydroperoxyl radicals through Fenton Reaction, which is the primary source of reactive oxygen species (ROS) to drive the damaging peroxidation chain reaction. Iron uptake via the transferrin receptor-like TfR1 or degradation of ferritin iron stores enhances the labile iron pool, thereby cells are susceptible to ferroptosis via lipid hydroperoxides generation. TfR1 encoded by *TFRC*, is a key cell surface molecule that regulates the uptake of iron-bound transferrin by receptor-mediated endocytosis [10]. Recently, TfR1 was reported to accumulate on the cell surface as a feature of ferroptosis [11]. However, the clathrin-mediated endocytosis is not disrupted during ferroptosis. Therefore, it remains enigmatic whether the posttranslational modification of TfR1 is involved in ferroptosis, especially under pathological conditions.

HUWE1 (also known as MULE, HectH9, ARF-BP1, URE-B1, and LASU1) is a crucial member of HECT domain E3 ligase family in eukaryotes [12]. HUWE1 regulates the turnover of numerous disparate substrates such as MCL-1, P53 and c-MYC, therefore participating in diverse biological processes, including but not limited to apoptosis, autophagy, proliferation, differentiation, DNA damage repair, and stress response [13–18]. Although loss of HUWE1 protects cells from DNA damage and histone deacetylase inhibitor-induced apoptosis

¹Key Laboratory of Cell Differentiation and Apoptosis of the Chinese Ministry of Education, Department of Pathophysiology, Shanghai Jiao Tong University School of Medicine, Shanghai 200025, China. ²Department of Liver Surgery, Renji Hospital, Shanghai Jiao Tong University School of Medicine, Shanghai 200127, China. ³Department of Nephrology, Renji Hospital, Shanghai Jiao Tong University School of Medicine, Shanghai 200127, China. ⁴Princess Margaret Cancer Centre, University Health Network, Toronto, ON M5G 2C1, Canada. ⁵Department of Biochemistry and Molecular Cell Biology, Shanghai Key Laboratory for Tumor Microenvironment and Inflammation, Key Laboratory of Cell Differentiation and Apoptosis of the Chinese Ministry of Education, Shanghai Jiao Tong University School of Medicine, Shanghai 200025, China. ⁶These authors contributed equally: Yan Wu, Huike Jiao, Yangbo Yue and Kang He. ✉email: yangbo.yue@outlook.com; xiaqiang@shsmu.edu.cn; qingzhong@shsmu.edu.cn; jingzhang@shsmu.edu.cn
Edited by C Borner

[12, 15], targeted deletion of *Huwe1* in the pancreas preferentially activated p53-mediated beta cell death *in vivo*, leading to reduced beta cell mass and diminished insulin exocytosis [19]. So far, little is known about the role of *Huwe1* in a variety of pathological conditions with massive cell death, such as hepatic ischemia/reperfusion and drug-induced liver injury.

In the present study, we unveiled the suppressive role of HUWE1 on ferroptosis *in vitro* and *in vivo*. *Huwe1* deficiency promotes ferroptotic cell death *in vitro* and exacerbates ferroptosis in acute liver injury *in vivo*. This is achieved by less TfR1 ubiquitination and stabilization upon the loss of HUWE1, leading to the dysregulation of iron metabolism. Importantly, expressions of HUWE1 in human donor liver biopsies negatively correlated with hepatic damage and tissue lipid peroxidation after liver transplantation in the patients. These findings contribute to our understanding of the intracellular mechanisms of ferroptosis in acute liver injury, especially in ischemia/reperfusion. Therefore, the HUWE1-TfR1 axis may be a potential therapeutic target for pharmaceutical agents that involving ferroptotic cell death in acute liver injury.

RESULTS

High expression of HUWE1 correlates with less hepatic injury in liver transplantation patients

Emerging evidence propose HUWE1/MULE as a critical ubiquitin ligase in the center of cellular response to multiple cell death pathways [12, 15, 20]. We aim to study the possible role of HUWE1 in oxidative stress induced cell death. Liver transplantation (LT) includes ischemia/reperfusion process since the blood supply of donor liver is artificially restricted (ischemia) before transplantation and restored (reperfusion) after transplantation. Therefore, we first evaluated the peri-operative graft expression of HUWE1 in a human liver transplantation cohort and collected obtained 14 pairs of pre-LT and post-LT liver biopsies. The protein level of post-LT HUWE1 was significantly decreased after reperfusion ($n = 14$, Fig. 1A, B). In parallel, we obtained another 11 pairs of pre-LT and post-LT liver biopsies to detect HUWE1 mRNA expression and 6 pairs for formalin fixation and paraffin embedding. The RNA levels of post-LT HUWE1 was significant downregulated in 9 out of 11 hepatic biopsies after reperfusion (Fig. 1C). Furthermore, immunohistochemistry results revealed remarkable decrease of HUWE1 in the hepatocytes after reperfusion (Fig. 1D). Additionally, hepatic I/R model was successfully established in mice, and *Huwe1* protein expression was measured in the liver samples. As shown in Fig. 1E, F, 90 min of portal vein blockage and subsequent reperfusion triggered a significant decrease of *Huwe1* in the liver. These observations suggest that hepatic I/R injury leads to the downregulation of HUWE1.

Next, we evaluated the correlation between pretransplant (pre-LT) HUWE1 levels and post-liver transplant (post-LT) hepatic damage in human LT patients ($n = 27$). According to the quantification of HUWE1 blots and based on the quantified mean value, the liver donor biopsies were divided into two groups: low and high HUWE1 expression (the mean value = 0.5172, Fig. 1G, H). These two groups had similar donor characteristics, donor serum transaminases and cold ischemia time (Supplemental Table 1). After reperfusion, we observed less tissue lipid peroxidation in the LT patients with pre-LT high expression of HUWE1 as detected by malondialdehyde (MDA), a byproduct of polyunsaturated fatty acid peroxidation (Fig. 1I). In line with this observation, serum transaminases (alanine aminotransferase, ALT; aspartate aminotransferase, AST) were significantly lower in the pre-LT high HUWE1 group, suggesting less injury and better hepatic function after liver transplantation (Fig. 1J). Of note, there was no significance between the HUWE1 high expressed group and HUWE1 low expressed group regarding to the rejection insults 1 year after liver transplantation surgeries (Supplemental Table 2).

Together, these data imply HUWE1 may play a role in the hepatic I/R injury.

Both the protein and mRNA levels of HUWE1 were downregulated after hepatic I/R injury in the patients, suggesting that HUWE1 is transcriptionally downregulated. Previous studies demonstrated that HUWE1 is a direct target of miR-542-5p in osteosarcoma cell lines, and was negatively correlated with miR-542-5p levels in human osteosarcoma tissues [21]. Moreover, it was reported hypoxia/reoxygenation upregulated miRNA-542-5p [22]. It's well known that hepatocytes suffer hypoxia/reoxygenation (H/R) in hepatic I/R injury. Therefore, we tested whether the downregulation of HUWE1 after hepatic I/R injury is due to the upregulation of miRNA-542-5p. miRNA-542-5p was indeed induced 3 h after I/R, and in the meantime, *Huwe1* was interestingly downregulated at mRNA level (Supplementary Fig. 1A, B). To mimic *in vivo* I/R injury, *in vitro* experiments were performed by treating primary hepatocytes with hypoxia/reoxygenation. Consistently, the expression of *Huwe1* became less at both protein and mRNA levels when exposed to H/R (Supplementary Fig. 1C, D). Moreover, we observed that miRNA-542-5p was increased after H/R in the primary hepatocytes (Supplementary Fig. 1E). Upon the specific inhibitor against miRNA-542-5p, HUWE1 mRNA was remarkably enhanced (Supplementary Fig. 1F). At the same time, HUWE1 protein was accumulated upon miRNA-542-5p inhibitor in primary hepatocytes (Supplementary Fig. 1C). Collectively, these data suggest that the induction of miR-542-5p upon I/R or H/R treatment is associated with the downregulation of *Huwe1*, and miRNA-542-5p at least are partially involved in the downregulation of HUWE1 during I/R.

Loss of *Huwe1* in hepatocytes exacerbates ferroptosis in acute liver injury in mice

The negative correlation between HUWE1 expression and hepatic damage post liver transplantation promoted us to hypothesize a crucial participation of HUWE1 in acute liver injury, especially in hepatic I/R insult. To further confirm the participation of HUWE1 in acute liver injury, we developed *Huwe1* ablation in a hepatocyte-specific manner, since the global *Huwe1* deficiency leads to early embryonic lethality [23]. We bred conditional *Huwe1*-flox mice with albumin-cre transgenic mice in which cre recombinase is under control of albumin promoter expressed efficiently and specifically in the liver (Fig. 2A). Liver I/R surgery and intraperitoneal injection with Carbon Chloride (CCl_4) were performed in *Huwe1* hepatocyte-specific knockout (HKO) mice and their control littermates. *Huwe1* knockout in the liver did not cause liver damage under normal conditions. As expected, hepatic I/R caused liver damage in both *Huwe1* WT and HKO mice at 6 h, as evidenced by the necrotic areas and elevated serum aminotransferases ALT and AST activities (Fig. 2B, C). Histological analysis revealed that *Huwe1* deficiency dramatically enlarged the necrotic area compared with the wildtype littermate controls at 6 h and even 24 h after I/R (Fig. 2B). Notably, *Huwe1* HKO mice exhibited much higher ALT and AST activities than WT mice at 6 h post-reperfusion, while both ALT and AST dramatically declined in *Huwe1* WT and HKO mice 24 h post-reperfusion (Fig. 2C). Moreover, TUNEL staining was performed to detect the cell death on the ischemic liver lobe sections. The number of TUNEL-positive cells was significantly increased in liver sections of *Huwe1* LKO mice at both 6 and 24 h after reperfusion (Fig. 2D, E). These data demonstrated exacerbated liver damage in the HKO group. In CCl_4 -induced acute liver injury, the liver damage in the HKO group was much higher than in the WT group 12 and 24 h after CCl_4 injection (Fig. 2F, G). More tremendous hepatocytes were injured in *Huwe1* HKO mice 12 and 24 h after CCl_4 compared to WT mice from TUNEL staining (Fig. 2H, I). These observations suggest that *Huwe1* plays a protective role in hepatic injury in response to I/R and CCl_4 .

It is generally believed that CCl_4 toxicity results from the bioactivation of the CCl_4 molecule to the trichloromethyl free

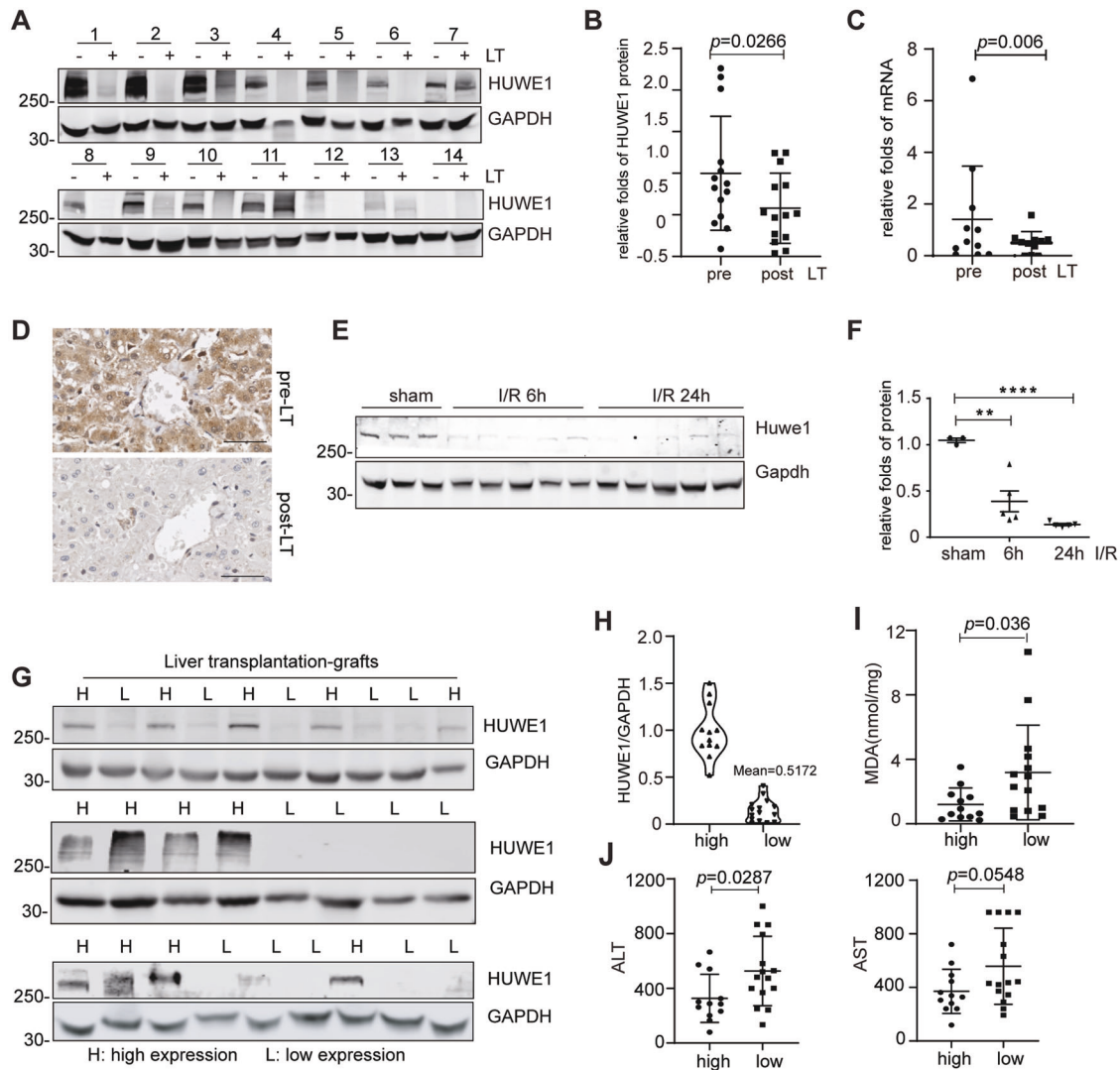
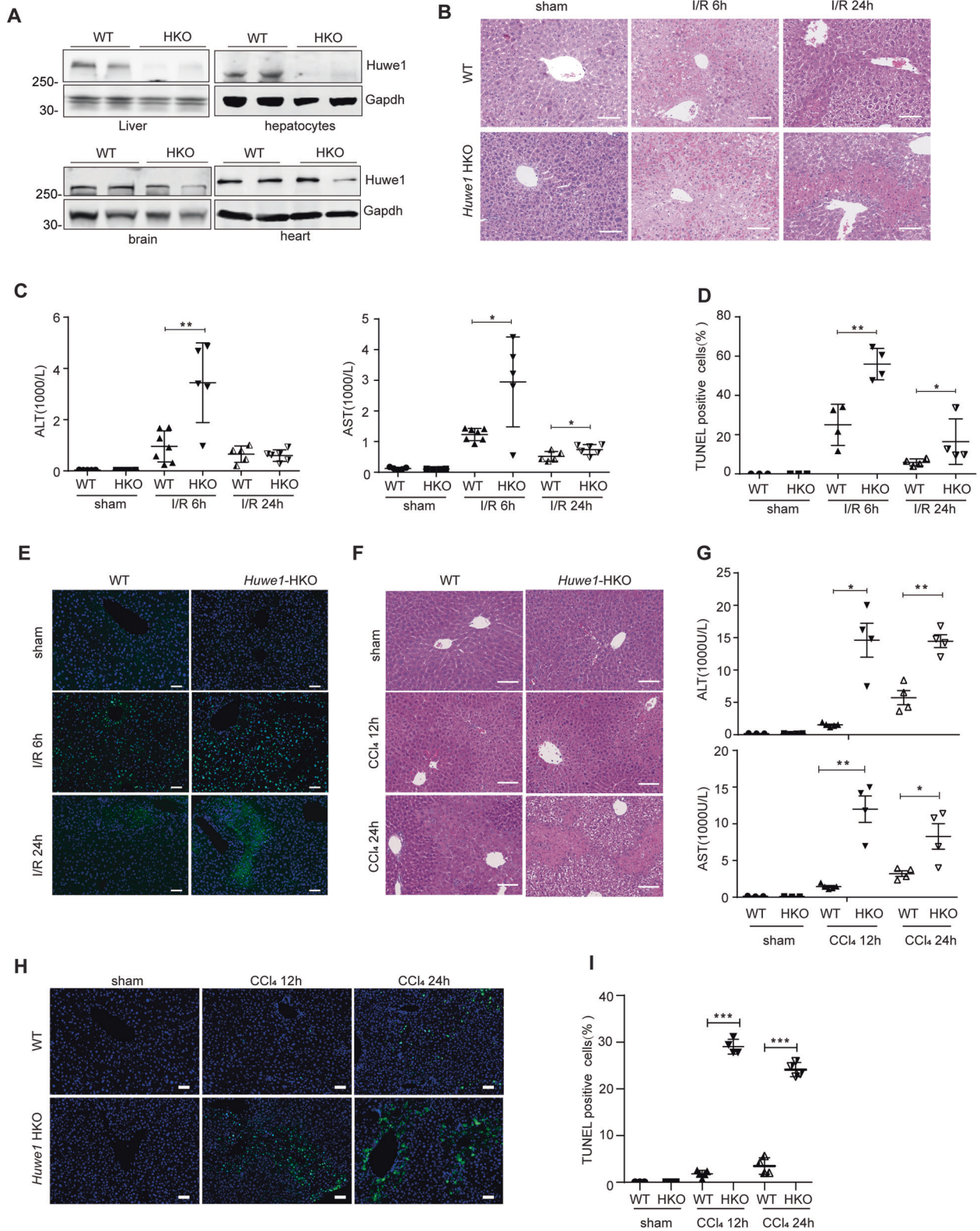


Fig. 1 High expression of HUWE1 correlates with less hepatic injury in liver transplantation patients. **A, B** The peri-operative graft expression of HUWE1 protein levels were detected from a human liver transplantation (LT) cohort (**A**, $n = 14$). (**B**) Protein levels of HUWE1 were normalized to those of GAPDH (pre-LT: 1 ± 0.68 vs post-LT: 0.58 ± 0.42). **C** HUWE1 mRNA levels in hepatic biopsies from another human liver transplantation cohort ($n = 11$, pre-LT: 1.41 ± 2.06 vs post-LT: 0.50 ± 0.44). **D** Immunohistochemistry of HUWE1 in hepatic biopsies from a human liver transplantation cohort ($n = 6$). Scale bar, 50 μm . **E, F** Huwe1 protein levels in the livers of mice subjected to 90min of ischemia and subsequent reperfusion for 6 or 24 h. Gapdh served as a loading control. $n = 3$ -5 per time point. Huwe1 protein levels were normalized to those of Gapdh (**F**). **G–J** From a human liver transplantation cohort ($n = 27$), HUWE1 expression was detected by Western Blots in donor liver samples (**G**). Pre-LT HUWE1 was analyzed with normalization to GAPDH (**H**). MDA were detected in LT recipients' liver biopsies (**I**, high: 1.21 ± 1.02 vs low: 3.19 ± 2.94). **J** The peak serum ALT (left) and AST (right) were measured within 48 h in LT recipients after liver transplantation (ALT, high: 326.3 ± 176 vs low: 526.9 ± 253.8 ; AST, high: 463.4 ± 206.3 vs low: 696.5 ± 354.9). The error bars represent the standard deviation of the indicated dataset. p value in (**B**) and (**C**) was analyzed by paired Student's t test (Prism; GraphPad) and the rest was analyzed by unpaired two-tailed Student's t test. $**p < 0.01$, $****p < 0.0001$ compared with sham group.

radical by cytochrome P450 isozymes such as cytochrome P450 2E1 (CYP2E1). No significant liver injury was observed in Cyp2e1^{-/-} mice when compared to wild-type counterparts after CCl₄ exposure [24]. To address whether lack of Huwe1 would affect CCl₄ metabolism, we detected the protein and RNA levels of Cyp2e1 in *Huwe1* WT and HKO mice upon CCl₄ treatments (Fig. 3A–C). The expression of Cyp2e1 protein was comparable, and even less in *Huwe1* HKO mice (Fig. 3A, B). Moreover, no significant difference was observed at the RNA level of Cyp2e1 between *Huwe1* WT and HKO mice (Fig. 3C). Besides, Cyp2e1 was degraded during the process of CCl₄-induced hepatotoxicity in both *Huwe1* WT and HKO livers, which was consistent with previous reports [24]. Therefore, Huwe1 deficiency in the liver did not affect CCl₄ metabolism.

Cell death during acute liver injury is a marked feature of, and a direct contributor to liver damage. Apoptosis in *Huwe1* HKO mice, as detected by cleaved Caspase-3, was comparable to and even less than that in WT mice induced by CCl₄ treatment (Supplementary Fig. 2A). Moreover, phospho-mixed lineage kinase domain-like pseudokinase (MLKL), the hallmark of necroptosis, was similar in the WT and *Huwe1* HKO groups (Supplementary Fig. 2B). We detected several known substrates of Huwe1 such as Mcl-1, Mfn2 and C-Myc, and didn't observe obvious changes between *Huwe1* HKO and WT groups (Supplementary Fig. 2C). Therefore, we hypothesize that Huwe1 may involve in other forms of cell death. To our surprise, increased expression of acyl-CoA synthetase long chain family member 4 (*Acsl4*) was observed in *Huwe1* HKO mice compared to WT mice in response to I/R, which



is consistent in CCl₄ treatment (Fig. 3A, D, Supplementary Fig. 2C). As reported, *Acs14* predicts the sensitivity of cancer cells to ferroptosis and is recognized as a biomarker of ferroptosis [8, 25, 26]. Glutathione peroxidase 4 (GPX4) was the first identified central inhibitor of ferroptosis, while in some other situations, alternative mechanisms exist to suppress ferroptosis such as

apoptosis-inducing factor mitochondria-associated 2 (AIFM2, also known as FSP1) and DHODH which is independent of GPX4. Gpx4 was reduced in *Huwe1* HKO mice subjected to I/R (Fig. 3A, left); and Fsp1 was simultaneously suppressed in *Huwe1* HKO mice in response to CCl₄ treatment (Fig. 3A, right), both of which implied more ferroptosis in *Huwe1* HKO mice in acute liver injuries.

Fig. 2 **Loss of Huwe1 in hepatocytes exacerbates acute liver injury in mice.** **A** Huwe1 protein levels in major organ samples from WT and hepatocyte-specific *Huwe1* HKO mice. $n = 2$. Gapdh served as the loading control. **B** The representative H&E staining of liver sections from WT and *Huwe1* HKO mice in the sham and I/R groups at 6 h and 24 h post-reperfusion. Scale bar, 100 μm . $n = 5-7$ for each time point. **C** Serum ALT (left) and AST (right) levels in WT and *Huwe1* HKO mice at 6 h and 24 h after I/R injury. **D-E** The statistical quantification of TUNEL-positive cells (**D**) and the representative images of TUNEL staining (**E**, scale bar = 50 μm) in liver sections of *Huwe1* WT and LKO mice 6 or 24 h after I/R. **F-I** WT and *Huwe1* HKO mice were intraperitoneally injected with 5% CCl_4 at 300 $\mu\text{l}/\text{kg}$ body weight for 12 and 24 h. **F** The representative H&E staining of liver sections from WT and *Huwe1* HKO mice in the sham and CCl_4 groups post CCl_4 injection for 12 or 24 h. Scale bar, 100 μm . $n = 5-6$ for each time point. **G** Serum ALT (up) and AST (bottom) levels in WT and *Huwe1* HKO mice at 12 or 24 h after CCl_4 injection. **H, I** Representative images of TUNEL staining (**H**) and the statistical quantification of TUNEL-positive cells (**I**). Scale bar = 50 μm . * $p < 0.05$, ** $p < 0.01$ compared with sham group by unpaired two-tailed Student's *t*-test.

Moreover, we measured several other putative biomarkers of ferroptosis in vivo, including lipid peroxidation-derived 4-hydroxynonenal (4-HNE) staining and tissue MDA content [27–29]. *Huwe1* HKO mice showed significantly higher levels of 4-HNE in response to I/R and CCl_4 compared to control mice (Fig. 3E, F). Increased hepatic MDA content was observed in *Huwe1* HKO mice subjected to I/R and CCl_4 challenge compared with their respective control groups (Fig. 3G). Given the important pathological feature of inflammation in necrosis [30], we detected the inflammatory response in acute liver injury. Remarkably, the mRNA levels of cytokines quantified by real-time PCR demonstrated that *Huwe1* deficiency enhanced the expression of pro-inflammatory cytokines (TNF α , IL6 and IL-1 β) induced by I/R and CCl_4 (Fig. 3H, I). In summary, these results demonstrated that loss of *Huwe1* in hepatocytes exacerbates ferroptosis in acute liver injury.

Huwe1 is a negative ferroptosis modulator

Previous reports demonstrated ferroptosis inhibitors Ferrostatin-1 and Liproxstatin-1 attenuated I/R-induced acute liver injury [31]. However, it's currently unknown if ferroptosis is also involved in CCl_4 induced liver injury. We observed that the exacerbated liver damage in the HKO group was remarkably alleviated by Ferrostatin-1, as measured by ALT/AST activities and histological analysis, suggesting ferroptosis is involved in CCl_4 induced liver injury (Fig. 4A, B and Supplementary Fig. 2D). To visually evaluate the function of *Huwe1* in hepatocytes, primary hepatocytes were isolated from the livers of *Huwe1* HKO mice and their littermate controls, then subjected to RSL3 or CCl_4 challenge. We observed profoundly augmented cell death in primary hepatocytes of *Huwe1* HKO mice by increased concentrations of RSL3 treatment, which could be rescued by Ferrostatin-1 (Fig. 4C and Supplementary Fig. 3A). Minor cell death was observed in WT primary hepatocytes in response to CCl_4 , however, cell death was significantly enhanced by *Huwe1* deficiency (Fig. 4C). Moreover, the enhanced cell death in *Huwe1* HKO hepatocytes induced by CCl_4 was remarkably blocked by ferroptosis inhibitor Ferrostatin-1 (Fig. 4D and Supplementary Fig. 3B), suggesting ferroptosis is involved in CCl_4 induced cell death in primary hepatocytes.

To validate the roles of *Huwe1* in ferroptosis, we treated *Huwe1* WT and KO MEFs with different ferroptosis inducers. Compared to wildtype cells, *Huwe1* KO MEFs were much more sensitive to RSL3 induced ferroptosis, while remained resistant to apoptosis induced by Cisplatin as reported (Fig. 4E, Supplementary Fig. 3C, D). It should be noted that the enhanced cell death in *Huwe1* KO MEFs was abrogated by specific ferroptosis inhibitors Ferrostatin-1, Liproxstatin-1, and iron chelator Deferoxamine (DFO), but neither the apoptosis inhibitor Z-VAD-FMK nor autophagosome-lysosome inhibitor chloroquine (CQ) (Fig. 4F). Therefore, the sensitized cell death triggered by RSL3 in *Huwe1* KO MEFs is indeed ferroptosis. As we know, there are four classes of typical ferroptosis inducers according to their impacts on ferroptosis and functional targets. Class I acts by inhibiting system x_c^- and reducing the intracellular glutathione content (eg. erastin); Class II works by inhibiting GPX4 directly (eg. RSL3 and ML210); Class III can reduce GPX4 protein abundance and simultaneously cause depletion of mevalonate-

derived coenzyme Q₁₀ (CoQ₁₀) (eg. FIN56); Class IV ferroptosis inducer FINO2 oxidizes ferrous iron, indirectly inactivate GPX4 and further drive lipid peroxidation [32]. According to our exploration, *Huwe1* KO remarkably amplified ML210, FIN56, and FINO2 induced cell death in MEFs (Fig. 4G). In addition, tertiary-butyl hydroperoxide (t-BuOOH) is a widely used oxidative stress inducer, which could be inhibited by ferroptosis inhibitors Ferrostatin-1 and Liproxstatin-1 [33, 34]. Here we found t-BuOOH induced cell death was also boosted by inhibition of *Huwe1* expression in MEFs (Supplementary Fig. 3E).

In the meantime, we analyzed events known to be critical for ferroptosis execution, such as mitochondrial morphology changes and lipid peroxidation [4, 35]. Studies of Electron Microscopy in *Huwe1* KO cells revealed shrunken mitochondria with increased membrane density (Fig. 4H). Next, we estimated lipid peroxidation in *Huwe1* WT and KO MEF cells using the lipid peroxidation-sensitive dye BODIPY 581/591 (C11-BODIPY) [4]. Although BODIPY is rarely oxidized in WT cells upon low dose of RSL3, massive lipid peroxidation was detected in *Huwe1* KO cells upon the same dose of stimulation (WT 3.17% \pm 2.08% vs KO 24.0% \pm 12.03%) (Fig. 4I).

To further confirm the role of *Huwe1* in ferroptosis, we knocked down *Huwe1* by specific shRNA in mouse hepatic carcinoma cell line Hepa-1c1c7 and obtained 2 stable knockdown cell lines (Fig. 4J). As detected by CellTiter Glo assay, Hepa-1c1c7 cells with suppression of *Huwe1* exhibited much more ferroptosis upon RSL3 treatment (Fig. 4J). Utilizing Sytox Green, a useful dye for dead cells which only penetrates the compromised membranes but not the intact membranes of the live cells, we observed massive dead cells with positive Sytox Green staining in *Huwe1* KD cells upon RSL3 treatment (Fig. 4K, Supplementary Fig. 3F, G). Moreover, lipid peroxidation was highly induced in *Huwe1* KD cells in response to RSL3, measured by flow cytometry using the fluorescent probe C11-BODIPY (Fig. 4L). Moreover, over-expression of *Huwe1* conferred cellular resistance to RSL3-induced ferroptosis in Hepa-1c1c7 cells (Supplementary Fig. 3H). Taken together, these findings demonstrate that *Huwe1* is a negative regulator of ferroptosis.

HUWE1 ubiquitinates and degrades Tfr1

To explore the underlying mechanism of *Huwe1* in ferroptosis, we screened interacting proteins using immunoprecipitation linked mass spectrometry (IP/MS) analysis (Supplementary Fig. 4A). The proteins pulled down by Flag-HUWE1 included MCL-1, USP7 and DDIT, which are well-known HUWE1 interacting proteins [12, 36] (Supplementary Fig. 4A). It should be noted that Tfr1 also existed in the pull-down list, which has previously been reported to involve in iron metabolism and ferroptosis as well [37, 38]. Therefore, we decided to use Tfr1 as a bait for the affinity proteomics reciprocally. As expected, HUWE1 together with ubiquitin was identified as Tfr1 interacting partners (Supplementary Fig. 4B). To verify the potential interaction between HUWE1 and Tfr1, we carried out co-immunoprecipitation assays in HEK293T cells and mouse liver hepatoma Hepa-1c1c7 cells. Tfr1 reciprocally interacted with HUWE1 in HEK293T cells (Fig. 5A and Supplementary Fig. 4C). Endogenous immunoprecipitation of Tfr1 co-precipitated *Huwe1* in Hepa-1c1c7 cells (Fig. 5B). These data confirmed the interaction between HUWE1 and Tfr1.

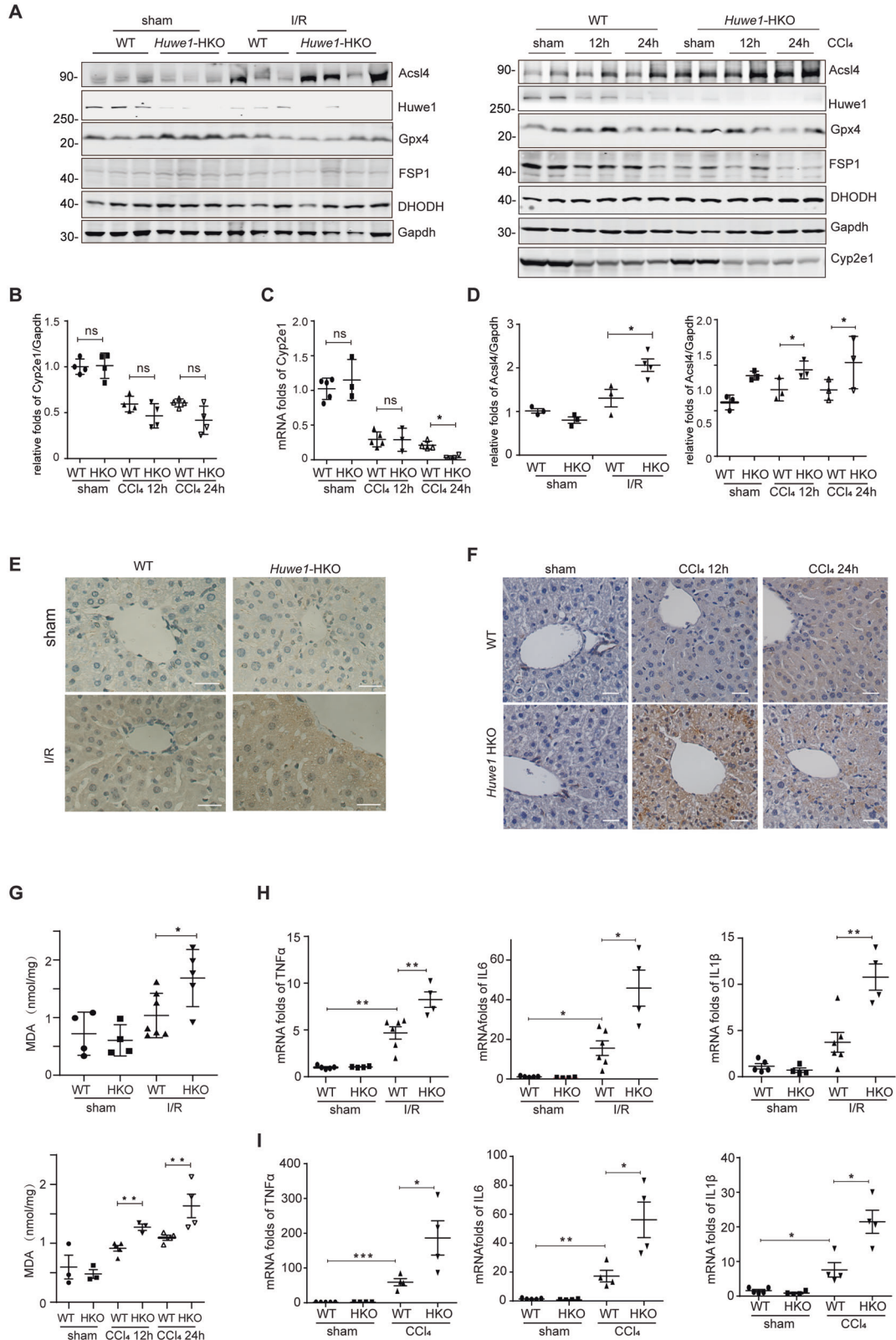
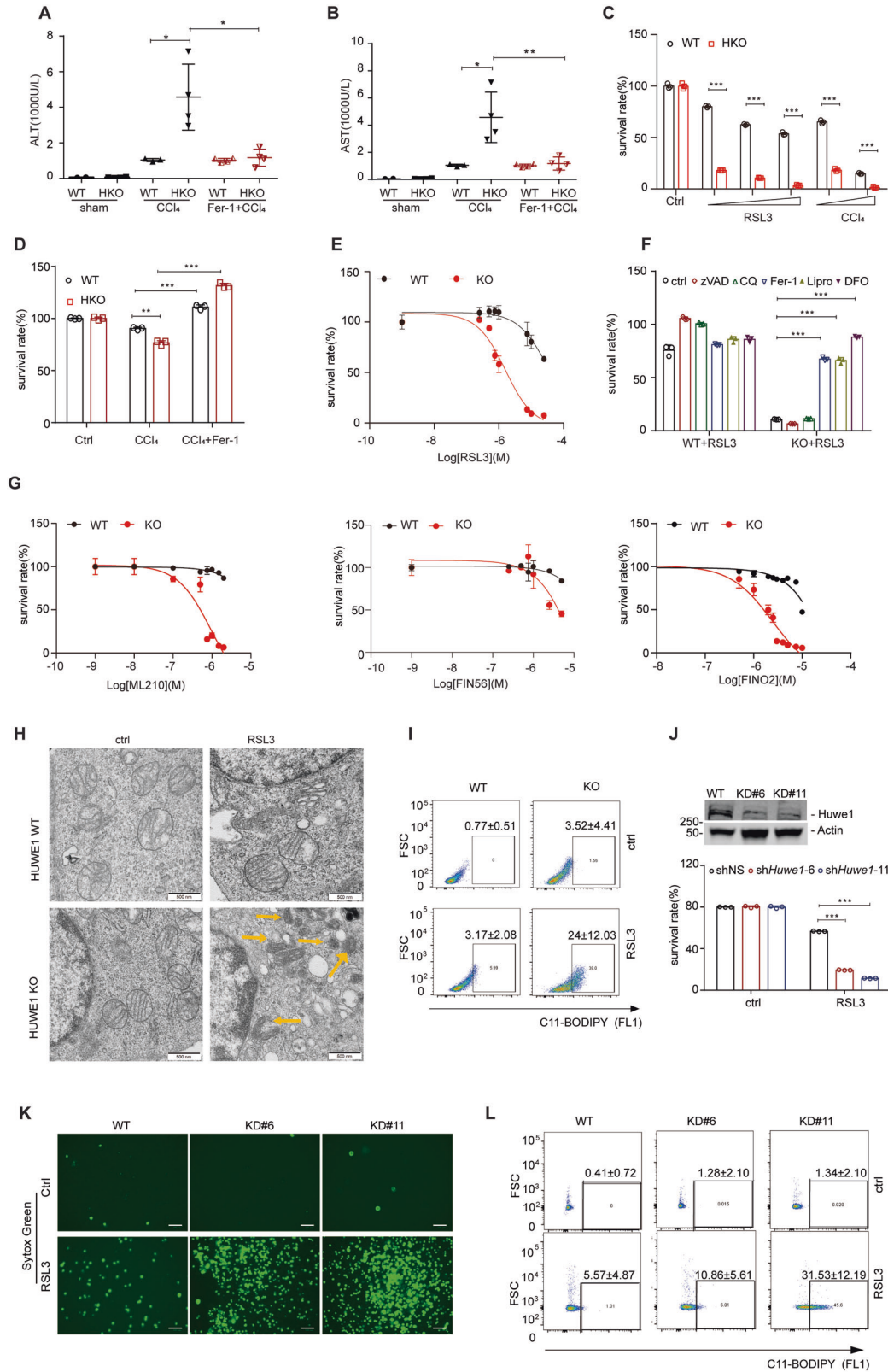


Fig. 3 **Huwe1** deficiency in hepatocytes aggravates ferroptosis in acute liver injury. WT and *Huwe1* HKO mice were subjected to I/R or CCl₄ injection. **A** Acs14, Gpx4, Fsp1, DHODH and Cyp2e1 were detected by western blotting, $n = 2-4$; **B** Cyp2e1 protein levels were normalized to those of Gapdh, $n = 3-4$. **C** The mRNA level of Cyp2e1 was determined by real-time quantitative PCR in WT and *Huwe1* HKO mice subjected to CCl₄ for 12 or 24 h. **D** Acs14 protein levels were normalized to those of Gapdh, $n = 3-4$. **E-F** Representative images of liver sections stained with 4-HNE in WT and *Huwe1* HKO mice subjected to I/R, **(E)** and CCl₄ for 12 or 24 h **(F)**. Scale bars, 50 μ m. **G** MDA levels were measured. $n = 3-5$. **H-I** mRNA levels of cytokines (TNF α , IL6 and IL1 β) in WT and *Huwe1* HKO liver lysates subjected to CCl₄ for 12 h **(H)** and I/R **(I)**. $n = 3-5$. * $p < 0.05$, ** $p < 0.01$, *** $p < 0.001$ compared in the indicated groups using unpaired two-tailed Student's *t*-test.



Considering the fact that ubiquitin was immunoprecipitated by TfR1 and that HUWE1 is a bona fide ubiquitin ligase (Supplementary Fig. 4B), we speculate that HUWE1 might influence the abundance of TfR1. As expected, HUWE1 overexpression decreased TfR1 protein levels in a dose-dependent manner (Fig. 5C). On the

contrary, TfR1 was accumulated in Huwe1 KO MEFs, while there was a minor decrease in TfR1 mRNA level in the absence of Huwe1 (Fig. 5D, E and Supplementary Fig. 4D). Furthermore, we observed that the half-life of TfR1 was extended to about 6 h in Huwe1 KO cells compared to less than 4 h in wildtype cells in the presence of

Fig. 4 Huwe1 is a negative ferroptosis modulator. **A, B** Fer-1 is dissolved in normal saline at 200 mg/ml for intraperitoneal injection in mice. WT and *Huwe1* HKO mice were pretreated by Ferrostatin-1 (Ferr-1) at 10 mg/kg body weight for 3 h before CCl_4 injection for 12 h, serum ALT (**A**) and AST (**B**) levels were measured. **C** WT and *Huwe1* HKO primary hepatocytes were isolated and cultured for overnight, then treated by 10, 20, 30 μM RSL3 or 0.125%, 0.25% CCl_4 , and cell viability was evaluated with CellTiter Glo. **D** Primary hepatocytes were isolated from *Huwe1* WT and HKO mice, treated by CCl_4 in the presence of Ferrostatin-1 (2 μM), and cell viability were detected. **E** *Huwe1* WT and KO MEFs were treated with gradient concentrations of RSL3 followed by cell viability analysis. **F** *Huwe1* WT and KO MEF cells were treated by RSL3 in the presence of Z-VAD-FMK (zVAD, 10 μM), Chloroquine (CQ, 2 μM), Ferrostatin-1 (Fer-1, 2 μM), liproxstatin-1 (lipro, 1 μM), or Deferoxamine (DFO, 100 μM), and cell viability were detected. **G** *Huwe1* WT and KO MEF cells were subjected to ML210, FIN56 or FINO2 treatments at indicated concentrations overnight, followed by CellTiter Glo assay. **H** Ultrastructural analysis of 1 μM RSL3-treated *Huwe1* WT and KO MEF cells for 2.5 h. Scale bars, 500 nm. Yellow arrows indicate shrunken mitochondrial with condensation. **I** BODIPY oxidation in *Huwe1* WT and KO MEF cells before and 3 h after 1 μM RSL3 treatment. **J–L** Knockdown of *Huwe1* sensitized ferroptotic cell death in hepatic carcinoma cell line Hepa-1c1c7. Immunoblotting of *Huwe1* for checking knock down efficiency by shRNA in hepatic carcinoma cell line Hepa-1c1c7 and cell survival rate was detected by CellTiter Glo (**J**) and Sytox Green staining (**K**, scale bar: 10 μm); Lipid peroxidation was analyzed by flow cytometry using C11-BODIPY in Hepa-1c1c7 cells with non-targeting or *Huwe1* shRNA upon RSL3 treatment (**L**). Data shown represent mean \pm SD from three independent experiments. * $p < 0.05$, ** $p < 0.01$, *** $p < 0.001$ compared in the indicated groups using unpaired two-tailed Student's *t*-test.

cycloheximide (CHX) to inhibit new protein synthesis (Fig. 5D). As previously reported, Tfr1 dynamic change is dependent on canonical endocytic machinery for its internalization, trafficking, sorting, lysosomal degradation or recycling to the plasma membrane [39]. Consistently, Tfr1 expression was accumulated by lysosome inhibitor CQ (Fig. 5E). Meanwhile, the proteasome inhibitor MG132 could also stabilize the intracellular Tfr1 suggesting that the ubiquitin-proteasome system is an important pathway for Tfr1 turnover (Fig. 5E). In line with this observation, Tfr1 protein was obviously accumulated in both primary hepatocytes with *Huwe1* knock-out and human hepatic carcinoma Huh7 cells with silencing of *Huwe1* by small interfering RNA (siRNA) (Fig. 5F and Supplementary Fig. 4E). Consistently, Tfr1 expression was higher in *Huwe1* HKO mice compared to their WT littermates. More Tfr1 were detected in *Huwe1* HKO mice subjected to CCl_4 and I/R (Fig. 5G, H and Supplementary Fig. 4F). These data suggest that HUWE1 controls Tfr1 protein stability.

To further confirm HUWE1 as an E3 ligase of Tfr1, we explored the ubiquitination of Tfr1 by HUWE1 in vivo and in vitro. HUWE1 overexpression enhanced Tfr1 ubiquitination, and the enhanced ubiquitination was further strengthened by MG132 (Fig. 5I). Then we purified the HECT domain of HUWE1 protein responsible for its ubiquitin ligase activity [15, 40]. In vitro ubiquitination assay indicated that, purified recombinant Tfr1 underwent dramatic ubiquitination in the presence of purified ubiquitin, E1, E2 (UbcH7), and the HECT domain of HUWE1, which was not seen when E1 and E2 were absent (Fig. 5J). To dissect the polyubiquitin chain linkage on Tfr1 catalyzed by HUWE1, ubiquitin mutants that contains arginine substitutions of all its lysine (K) residues except K48 was used in the transfection assays. HUWE1 markedly enhanced K48-linked polyubiquitination of Tfr1 (Fig. 5K). Together, these results suggest that Tfr1 is a direct substrate of HUWE1 for its ubiquitination and proteasomal degradation.

Huwe1 regulates iron metabolism

Given that Tfr1 mediates uptake of circulating transferrin-bound iron and plays a critical role in systemic iron homeostasis [37, 41], we assumed *Huwe1* might regulate iron metabolism. To test this hypothesis, we first examined the labile Fe(II) in response to RSL3 using a Fe(II)-selective probe RhoNox-1 [42]. While minor Fe^{2+} release in control cells was observed, massive Fe^{2+} leakage was detected in *Huwe1* KO MEF cells with RSL3 treatment (WT 8.93% \pm 6.15% vs KO 36.97% \pm 6.53%) (Fig. 6A). Consistently, we observed a higher level of ferrous ion after RSL3 treatment in *Huwe1* KO MEF cells indicated by FerroOrange staining (Fig. 6B). Perl's Prussian blue staining demonstrated that the deposition of free iron in *Huwe1* HKO livers was significantly increased in response to CCl_4 and I/R treatment compared to control group (Fig. 6C, D). To further confirm the role of *Huwe1* in iron metabolism, we fed the mice with a high-iron diet (HID) for

15 weeks, which is reported to induce ferroptosis in vivo [28]. No significant increase of ALT and AST were observed in *Huwe1* WT and HKO mice, which was consistent with previous studies (Supplementary Fig. 5A–C). Much more severe iron overload in the liver was detected in *Huwe1* HKO mice after HID diet feeding, as supported by more intense Perl's Prussian blue staining of liver sections (Fig. 6E). In addition, HID-fed *Huwe1* HKO mice exhibited higher iron content in homogenized liver tissues (Fig. 6F). Notably, compared with NID-fed control mice, HID-fed *Huwe1* HKO mice developed more severe ferroptosis, reflected by higher MDA levels and increased expression of *Acsl4* (Fig. 6G–I). Moreover, more Tfr1 was detected in the liver tissue of HID-fed *Huwe1* HKO mice (Fig. 6H and Supplementary Fig. 5D). Above all, these data proved the crucial role of *Huwe1* in iron metabolism.

Huwe1-mediated degradation of Tfr1 mitigates ferroptosis and acute liver injury

Although previous studies demonstrated Tfr1 is required for serum induced necrosis [43], the significance of HUWE1 modulated Tfr1 in ferroptosis still needs to be investigated. The small molecule compound Ferristatin II/NSC306711 was reported to promote the degradation of Tfr1 and inhibit iron uptake through the Tf-Tfr pathway [44]. We showed that Ferristatin II reversed the increased cellular sensitivity of *Huwe1* KO MEFs to RSL3-induced ferroptosis (Fig. 7A and Supplementary Fig. 6A). More specifically, *Huwe1* KO sensitized ferroptosis was significantly inhibited by *Tfrc* RNAi in the MEFs (Fig. 7B and Supplementary Fig. 6B). Furthermore, we generated stable cell lines that express shRNA against *Tfrc* in *Huwe1* KD Hepa-1c1c7 cells. Remarkably, lowering the Tfr1 level was sufficient to block the augmented cellular sensitivity to ferroptosis in Hepa-1c1c7 *Huwe1* KD cells (Fig. 7C and Supplementary Fig. 6C). These data indicate the significance of the HUWE1-Tfr1 axis in ferroptosis.

To further evaluate the physiological function of the HUWE1-Tfr1 pathway in mice, we carried out *Tfrc* loss-of-function in vivo. We forced to knockdown Tfr1 in the liver of mice using adeno-associated viruses (AAV) delivery intravenously with two pairs of shRNA targeting *Tfrc* and carried out I/R injury model after 4-week recovery (Supplementary Fig. 6D). It should be noted that there were no significant differences in the body weights between AAV-sh*Tfrc* and AAV-green fluorescent protein (GFP) injected mice (Supplementary Fig. 6E). Intriguingly, the aggravated liver damage after I/R in *Huwe1* HKO mice was blunted by Tfr1 suppression, as indicated by the size of the necrotic area (Fig. 7D) and the serum aminotransferase (ALT and AST) levels (Fig. 7E). Notably, performance of I/R-induced ferroptosis parameters including 4-HNE staining and *Acsl4* protein levels were much weaker in the *Huwe1* HKO, *Tfrc* KD mice, while *Huwe1* HKO mice still showed significantly higher 4-HNE and *Acsl4* in the liver compared to their respective control groups (Fig. 7F, G). *Tfrc* knockdown decreased

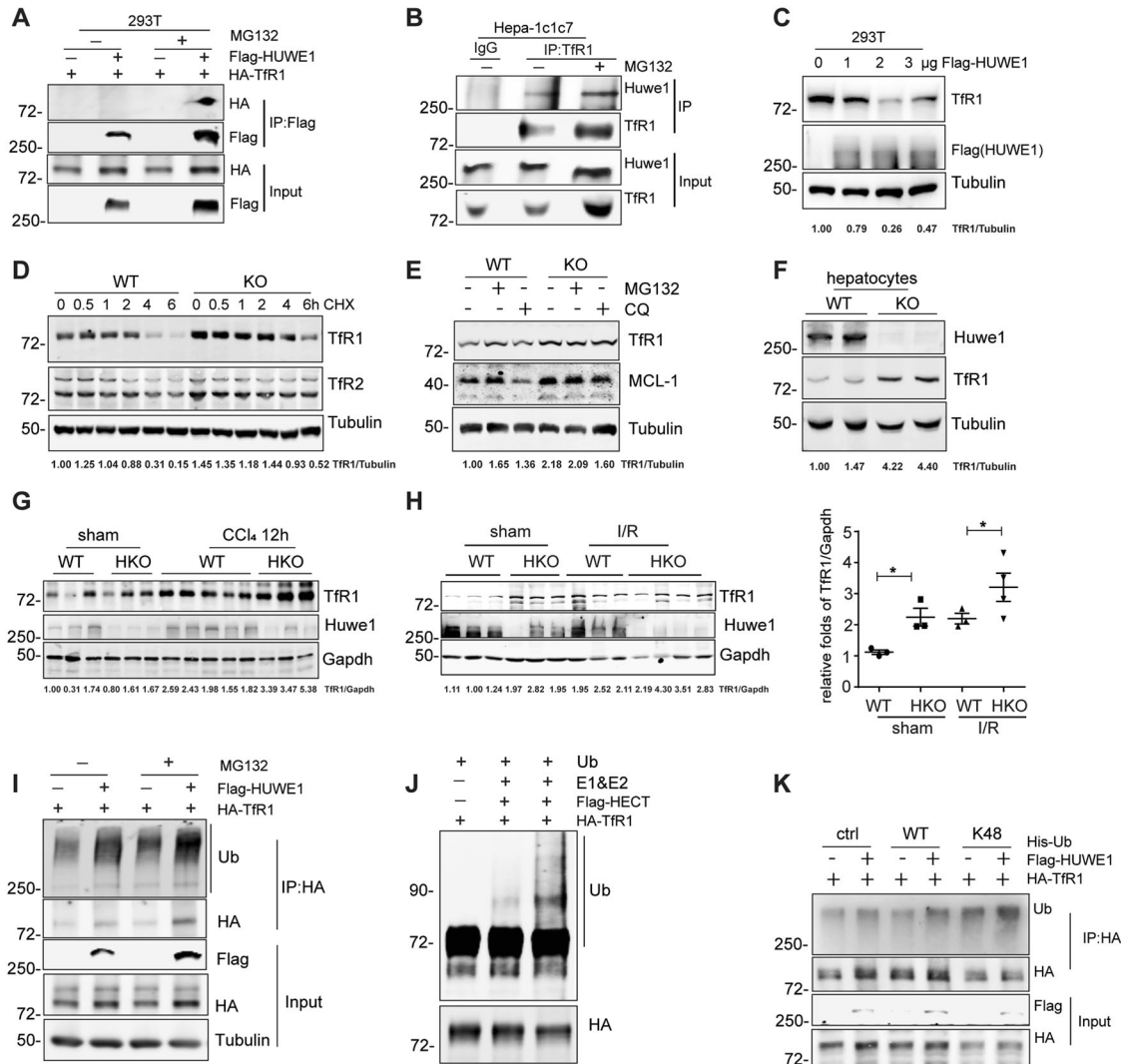


Fig. 5 HUWE1 ubiquitinates and degrades Tfr1. **A** Co-immunoprecipitation of HA-Tfr1 with Flag-HUWE1 in HEK293T cells. Exogenous HUWE1 was immunoprecipitated using Flag-M2 beads, and the immunoprecipitants were immunoblotted with HA antibody. **B** Co-immunoprecipitation of Huwe1 with Tfr1 in mouse liver hepatoma Hepa-1c1c7 cells. Endogenous Tfr1 was immunoprecipitated using anti-Tfr1, and the immunoprecipitants were immunoblotted with Huwe1 antibody. IgG, immunoglobulin G. **C** 293T cells were transfected with increasing levels of Flag-HUWE1, endogenous Tfr1 was detected by western blot. Huwe1 WT and KO MEFs were treated with 15 μg/ml cycloheximide (CHX) (**D**), 10 μM MG132 or 10 μM Chloroquine (CQ) (**E**), endogenous Tfr1 was immunoblotted. Mcl-1 was used as a positive control. **F** Immunoblotting of Huwe1 and Tfr1 in hepatocytes isolated from Huwe1 WT and KO mice. **G** Hepatic Huwe1 and Tfr1 were immunoblotted in *Huwe1* WT and HKO mice challenged by CCl₄ for 12 h. (**H**) Hepatic Tfr1 were detected by immunoblotting in *Huwe1* WT and HKO mice subjected to I/R for 6 h. Tfr1 protein levels were normalized to those of Gapdh. **p* < 0.05, compared to the indicated groups. **I** Ubiquitination of HA-Tfr1 in HEK293T cells co-expressed with empty vector or Flag-HUWE1 treated by MG132 for 4 h before harvesting. **J** Recombinant Tfr1 (100 nM) was incubated with ATP regenerating buffer, E1, E2, recombinant proteins of His tagged HECT domain of HUWE1 (10 nM, or 40 nM), and ubiquitin in a 30 μl reaction volume for 1 h at 37 °C. Three independent experiments were performed to confirm the ubiquitination of Tfr1 by HUWE1 in vitro. **K** Immunoprecipitation analysis from HEK293T cells transiently co-transfected with HA-Tfr1, Flag-HUWE1 and Wildtype or K48-Ubiquitin. The Tfr1 bands in **C–H** were quantified with the Image J software, and the ratio of Tfr1 to Tubulin or Gapdh in each lane was indicated on the bottom.

the higher iron content in *Huwe1* HKO mice in homogenized liver tissues after I/R (Supplementary Fig. 6F, G). Moreover, suppression of Tfr1 attenuated the elevated expression of pro-inflammatory cytokines in *Huwe1* HKO mice, including TNFα and IL6 (Fig. 7H, I). Thus, consistent with our in vitro results, these data indicate the significance of HUWE1-Tfr1 axis in hepatic I/R injury.

Finally, it's interesting to test whether the iron overload caused by HUWE1 conditional knockout is restricted to the liver. Previous studies demonstrated that the expression of HUWE1 was reduced in left ventricular samples from end-stage heart failure patients [45]. Specific ablation of Huwe1 in cardiomyocytes in mice dramatically decreased NADPH content and reduced

glutathione/oxidized glutathione (GSH/GSSG) ratios, which are key component in cellular anti-oxidation systems, leading to spontaneous cardiac hypertrophy, left ventricular dysfunction, and early mortality [45]. In line with these observations, we demonstrated that knock-down of HUWE1 in the rat cardiac myoblast H9C2 cells by siRNAs remarkably slowed down the proliferation of rat cardiac myoblasts (Supplementary Fig. 7A, B). Moreover, both lipid peroxidation and the labile iron pool at the basal level was mildly upregulated in HUWE1 knockdown H9C2 cells compared with the negative control (Supplementary Fig. 7C, D). Collectively, these evidences suggest HUWE1 deficiency in the cardiomyocytes leads to oxidative stress and enhanced labile iron pool.

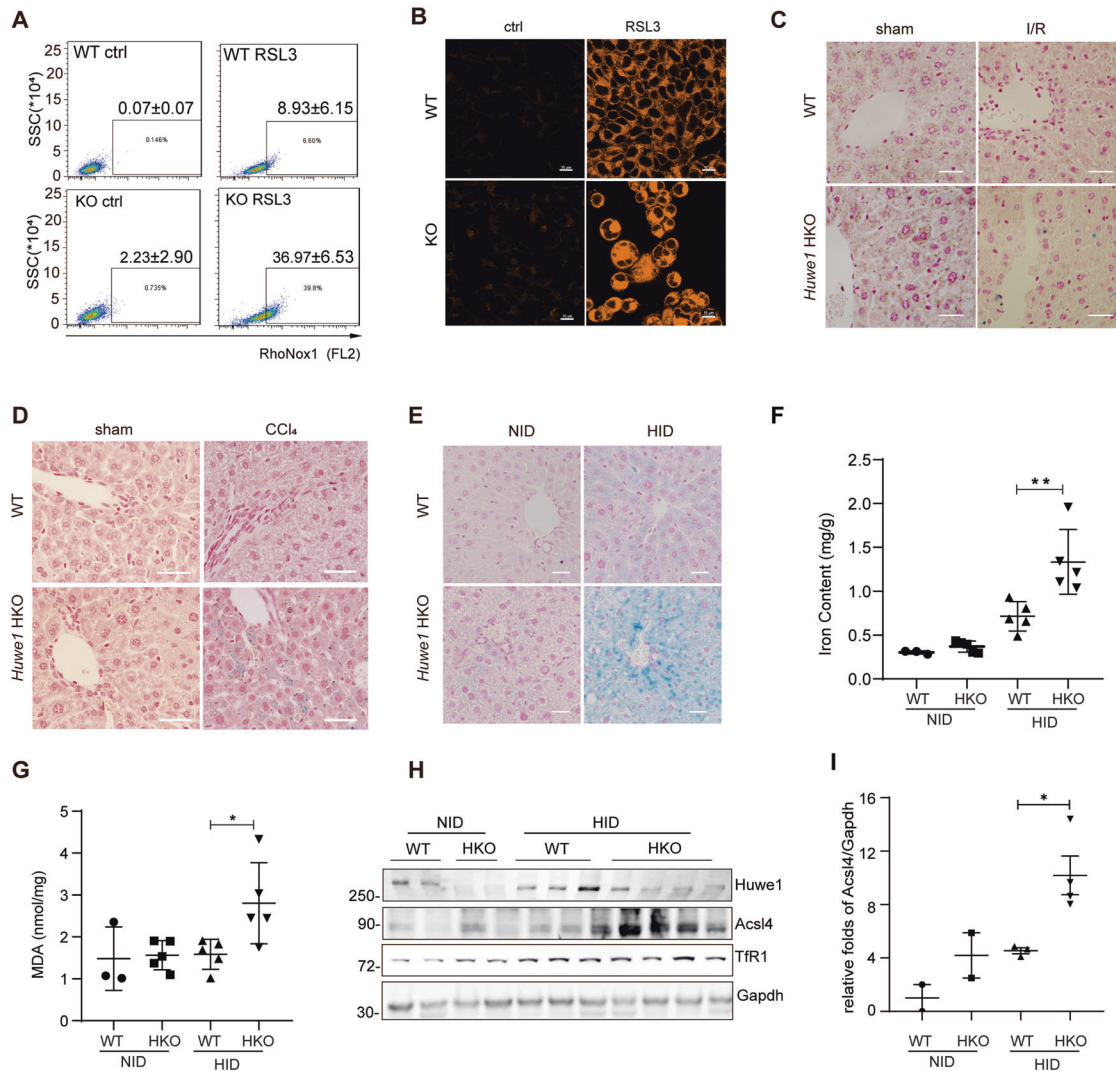


Fig. 6 **Huwe1 regulates iron metabolism.** **A** Cellular levels of labile Fe (II) detection. *Huwe1* WT and KO MEF cells were exposed to 1 μ M RSL3 for 2 h, stained with RhoNox-1, and analyzed by flow cytometry. **B** Confocal images of *Huwe1* WT and KO MEF cells treated by 1 μ M RSL3 for 2 h then labeled with FerroOrange. Scale bars, 10 μ m. The figures were representative of three different experiments. **C**, **D** Perl's Prussian blue staining of liver sections obtained from *Huwe1* WT and HKO mice after I/R (**C**, $n = 5-7$) or CCl_4 treatment for 12 h (**D**, $n = 5-6$). Scale bars, 50 μ m. *Huwe1* WT and HKO mice were fed with HID or NID for 15 weeks, Perl's Prussian blue staining (**E**), tissue iron content (**F**), MDA (**G**), immunoblots of *Acs14* and *Tfr1* of the liver sections (**H**) and the normalization of *Acs14* protein levels to those of *Gapdh* were analyzed (**I**). $n = 5$, scale bars represent 50 μ m. * $p < 0.05$, ** $p < 0.01$, *** $p < 0.001$ compared in the indicated groups using unpaired two-tailed Student's *t*-test.

DISCUSSION

The signaling pathway that participates in ischemic-reperfusion injury during liver transplantation are of crucial interests. In this study, we observed that HUWE1 negatively correlates with hepatic injury in liver transplantation patients and propose HUWE1 as a negative regulator of ferroptosis in acute liver injury (Graphical Abstract). Inhibition of *Huwe1* promotes ferroptosis in cells and acute liver injury mediated by CCl_4 or I/R in mice. Further mechanistic studies demonstrated that this regulation is achieved through maintaining regular iron metabolism by *Huwe1*, which specifically interacts with and targets *Tfr1* for degradation through K48-mediated ubiquitination. Inhibition of *Tfr1* blocked ferroptotic cell death in *Huwe1* KO cells and attenuated liver injury in *Huwe1* HKO mice.

It's intriguing that HUWE1 is involved in both pro-cell death and anti-cell death pathways. Although we reported that HUWE1 promotes DNA damage-induced apoptosis through degradation of anti-apoptotic MCL-1 [12, 15], deletion of HUWE1 in hepatocytes did not change MCL1 protein expression, suggesting that

MCL1 regulation is context-specific. Herein, we provided evidence that *Huwe1* deficiency in hepatocytes elaborated lipid peroxidation, ferroptotic cell death and liver damage through the accumulation of *Tfr1*, and proposed that *Huwe1* protects ferroptosis in acute liver injury. These findings suggest that HUWE1 can regulate substrates differently in specific settings, similar to the recent report on the dual role of HUWE1 in the regulation of B lymphocyte and pancreatic beta cells [19, 23]. Pancreas-specific *Huwe1* deletion led to increased beta cell death and reduced beta cell mass under basal conditions. In contrast, the same *Huwe1*-deficient mice protected against multiple-low-dose-streptozotocin-induced beta cell apoptosis and diabetes [19]. Another possibility of the complex role of HUWE1 on cell death may depend on p53. Inactivation of endogenous HUWE1 is crucial for p53 stabilization, which promotes apoptotic response [13]. On the other hand, activated p53 represses the expression of SLC7A11, thus inhibits cystine uptake and sensitizes cells to ferroptosis [46]. In some other cases, prolonged stabilization of wild-type p53 renders many cancer cells less sensitive to

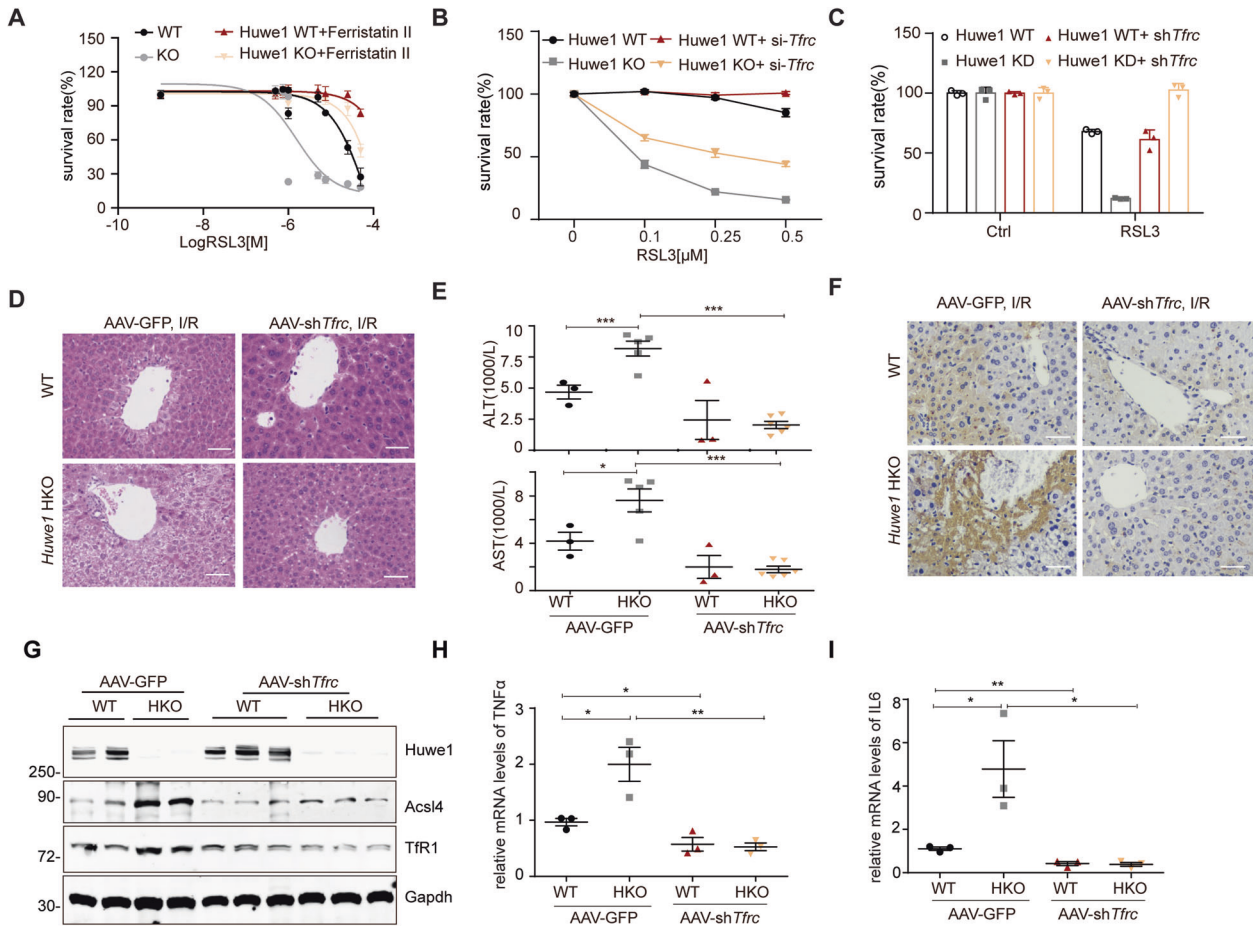


Fig. 7 Huwe1-mediated degradation of Tfr1 mitigates ferroptosis and acute liver injury. **A, B** Tfr1 inhibition protected against Huwe1 KO sensitized ferroptotic cell death. Huwe1 WT and KO MEFs were pretreated with Ferristatin II for 4 h (**A**) or transfected with siRNA against *Tfr1* for 36 h (**B**), then subject to different concentrations of RSL3 treatment. Cell viability was evaluated with CellTiter Glo. **C** Tfr1 was stably knocked down by shRNA in Huwe1 wildtype and knockdown Hepa-1c1c7 cells and then treated with RSL3. Cell viability was evaluated with CellTiter-Glo. All the data are representative of at least three independent experiments and presented as the means \pm SD. **D–I** AAV9-sh*Tfr1* and AAV9-GFP were injected in the lateral tail vein of *Huwe1* HKO and control mice to knock down *Tfr1* for 4 weeks, then mice were subjected to I/R surgery. Representative H&E staining images (**D**), serum ALT and AST levels (**E**), 4-HNE staining in the liver sections (**F**), and Acs14 expression (**G**) were evaluated 6 h after I/R injury in the indicated groups. $n = 3–5$. Scale bars, 50 μ m. Levels of cytokines (TNF α , IL6) in liver lysates were analyzed by real-time quantitative PCR (**H–I**, $n = 3–4$). Data and error bars are mean \pm s.d., $n = 3$ independent repeats in **A–C**. * $p < 0.05$, ** $p < 0.01$, compared in the indicated groups using unpaired two-tailed Student's *t* test.

ferroptosis induced by cystine deprivation through p53-p21 axis [47]. Of note, cardiac-specific Huwe1 knockout leads to severe oxidative stress, cardiomyocyte cell death and cardiac dysfunction, suggesting that HUWE1 might function similarly in cardiomyocytes. We recognize that further investigation is needed to clarify the direct contribution of iron overload to the cardiac dysfunction caused by loss of Mule.

In a clinical data of 202 pediatric living donor liver transplantation, a high level of serum ferritin was observed, which is considered as a marker of iron overload. These findings demonstrate that iron overload is a novel risk factor for hepatic I/R injury in LT, and ferroptosis contributes to the pathogenesis of hepatic I/R injury [31]. Tfr1 involves in cellular transport of iron into cells through binding of iron-loaded transferrin (Tf) [10]. The liver iron content is lower in *Tfr1* hepatocyte-specific knockdown mice compared with control littermates as a result of the reduced capacity of *Tfr1*-deficient hepatocytes to internalize iron from transferrin [37]. Cells with knockdown of Tfr1 are more resistant to serum-induced cell death, which was subsequently determined to be ferroptosis [43]. However, whether Tfr1 participates in ferroptosis in pathological conditions is not clearly characterized. In our studies, genetical or chemical suppression of Tfr1 efficiently

rescued enhanced ferroptosis in Huwe1 KO cells. Moreover, the degradation of Tfr1 is required for the protective role of Huwe1 in hepatic I/R injury. Therefore, it is of great significance to investigate whether targeting HUWE1-Tfr1 axis will ameliorate pathological injuries in which ferroptosis has been involved.

Tfr1 expression is finely regulated at multiple levels by distinct stimuli: Iron deficiency triggers transcriptional induction of Tfr1 via hypoxia-inducible factors [48, 49]. On the other hand, iron deficiency also leads to posttranscriptional stabilization of Tfr1 mRNA upon binding of iron-regulatory proteins (IRPs) to its iron-responsive elements [50]. At the post-translational levels, Tfr1 is degraded through clathrin-dependent endocytosis of iron-loaded transferrin. Previous work showed that membrane-associated RING-CH (MARCH) 8 ubiquitinates Tfr and promotes its lysosomal degradation [51]. However, the ubiquitination of Tfr2, another member of the transferrin receptor family as a homolog to Tfr1, seems not required for its degradation through endocytosis [52]. We observed Tfr1 accumulates treated by CQ, an autophagosome-lysosome inhibitor, supporting the notion that Tfr1 is recycled through the endosome-lysosome pathway. More importantly, our results revealed that the proteasome degradation of Tfr1 is a critical event for iron metabolism and ferroptosis. HUWE1 mediates

the interaction and ubiquitination of Tfr1, therefore, dampens the recycling of Tfr1 as well as the iron uptake.

In conclusion, we have identified HUWE1 as a novel ferroptosis suppressor in acute liver injury. HUWE1 targets Tfr1 for ubiquitination and degradation to modulate iron metabolism and thus ferroptosis. Our study provides experimental evidence that targeting HUWE1-Tfr1 axis as a novel strategy for clinical intervention of acute liver injury including I/R.

MATERIALS AND METHODS

Patients and liver biopsies

Human liver biopsies and serums were obtained from donors before liver graft resection (pre-LT) and recipients after liver transplantation (post-LT). Pre-LT hepatic biopsies were collected before graft removed from living donors and post-LT biopsies were obtained 3 h after reperfusion (prior to abdominal closure) following a standard protocol. Patients' serum alanine aminotransferase (ALT) and aspartate aminotransferase (AST) were measured within 48 h after liver transplantation to obtain the peak value using a standard clinical automatic analyzer (Dimension Xpand; Siemens Dade Behring, Munich, Germany). Samples were subject to western blotting, real-time quantitative PCR, immunohistochemistry (IHC), iron and MDA content measurement described below in details.

This study has been approved by the Institutional Review Board of Renji Hospital affiliated to Shanghai Jiao Tong University School of Medicine (IRB Reference Number: KY2020-190). The participants or their guardians provided signed consent.

Mice

Male WT C57BL/6 mice (8–10 weeks old) were purchased from Shanghai SLAC Co. Ltd (Shanghai, China). C57BL/6 *Huwe1^{Flox/y}* mice were kindly provided by Dr. Tak Wah Mak (University Health Network, Toronto, Canada). *Huwe1^{Flox}* mice were crossed with Albumin-cre mice (Jackson Laboratory, Bar Harbor, ME, USA) to generate *Huwe1* hepatocytes-specific knock out (*Huwe1* HKO). PCR-based genotyping was performed using the primer pairs as previously described [23]. All animals in the present study were bred in a standard environment with 12 h light/dark cycles and utilized for the experiments at the age of 8–10 weeks. All procedures related to animals were reviewed and approved by the Institutional Animal Care and Use Committee of Shanghai Jiao Tong University School of Medicine (Shanghai, China).

Chemicals and cell lines

Carbon tetrachloride (CCl₄), tert-butyl hydroperoxide (t-BuOOH), 1S,3R-RSL3, ML210, FIN56, and FINO2 were purchased from Sigma-Aldrich (St Louis, MO, USA). Ferrostatin-1, Deferoxamine (DFO) and Liproxstatin-1 were supplied by Selleck (Houston, TX, USA). Ferristatin II/NSC306711 was produced by MedChemExpress (Newark, NJ, USA). CCl₄ was freshly diluted with corn oil at the ratio of 1:19. Mice were given an intraperitoneal injection of 5% CCl₄ at 300 µl/kg body weight. All the other compounds were dissolved in Dimethyl Sulfoxide (DMSO) (Sigma-Aldrich) for cell culture-based experiments. For mice treatments, Fer-1 is dissolved in normal saline at 200 mg/ml and intraperitoneally injected at 10 mg/kg body weight 3 h before CCl₄ treatments.

Human embryonic kidney HEK293T and Hepa-1c1c7 cell lines were purchased from the American Type Culture Collection. *Huwe1* WT and KO mouse embryonic fibroblasts were described as previously [15]. Hepatocellular carcinoma cell lines Huh7 was a gift from Dr. Xuxu Sun at Shanghai Jiaotong University School of Medicine. These cell lines were maintained at 37 °C in a humidified incubator with 5% CO₂ and cultured in Dulbecco's modified Eagle's medium (DMEM, Sigma) supplemented with 10% FBS (Sigma-Aldrich) and 1% penicillin/streptomycin (Sigma-Aldrich). For all cell-based studies, cells were randomly assigned to different treatment conditions with three samples at least. Investigators were not blinded to the cell-free and cell-based experiments, because the measurements were quantitative and not subjective.

Plasmids, siRNA, shRNA and sgRNA

Tfr1 cDNA was purchased from the DNA library of Shanghai Jiao Tong University School of Medicine and was cloned into a modified pCDNA4 plasmid (Invitrogen, Carlsbad, CA, USA), with a C-terminal HA epitope [53]. HUWE1shRNA (sequence as 5'-CCGACTGTGTTAAACCAGAT-3') was cloned

into Tet-pLKO-puro (Addgene #21915). *Huwe1* sgRNA (sequence as 5'-GGACCUGUUGGACCGCUUCG-3') was cloned into lentiCRISPR-v2 (Addgene #52961). Three siRNAs targeting mouse Tfr1 (1# 5'-AGAGUCUCCUUCCGCAUUAU-3', 7# 5'-ACAGCAAUUGGAUUGCA A-3', 12# 5'-CCAGCCGUUAU-GUUGUAGUA-3') and non-targeting siRNA (5'-UUCUCCGAACCGUGACCGU TT-3') were synthesized by Shanghai GenePharma Co., Ltd (Shanghai, China). The same oligos were cloned into a modified Tet-pLKO-puro vector.

Animal treatments

For animal studies, animals were randomly assigned to specific treatment and control groups. Sample sizes were chosen to provide sufficient sample for common statistical test in animal study. Investigators were blinded to animal experiments. The experimental groups were injected intraperitoneally with 5% CCl₄ (Sigma-Aldrich) diluted in corn oil at 300 µl/kg body weight for indicated times, and littermates in the sham group were injected with corn oil.

Both standard AIN-76A diet containing 50 mg iron/kg normal iron diet (NID, Dyets, Bethlehem, PA, USA) and the high-iron diet (HID; 8.3 g carbonyl iron/kg) were egg white-based AIN-76A diets (Dyets). Mice were fed with NID or HID for 15 weeks and then sacrificed for analysis.

Hepatic I/R mice model and treatment

The model of warm partial hepatic I/R injury was used as described in previous study [54, 55]. In brief, the control group (sham) only had free hepatic portal blood vessels after laparotomy, and did not block blood flow. The hepatic I/R group was freed from the hepatic portal vein and the blood supply to the left lobe and mid-hepatic lobe was blocked for 90 min. Then the blood vessels were then opened for 6 h or 24 h. If the mice died before the sample collection, the regarded mice were discarded for analysis. All the operations were performed by the same operator.

AAV-shTfr1 production, purification, and injection

AAV9-U6 shTfr1 CMV-GFP was produced and purified by Hanbio Biotechnology Co. Ltd. (Shanghai, China) using sequence 5'-AGAGTCTC CTTCCGCATAT-3' and 5'-ACAGCAATTGGATTAGCAA -3' specifically targeting to Tfr1. For knocking down Tfr1 in vivo, the animals were injected in the lateral tail vein with a dose of 1.3×10^{11} genome copy (GC) of AAV9-shTfr1. A dose of 1.3×10^{11} GC of AAV9-GFP was injected into the lateral tail vein of control groups. After 4 weeks of recovery, I/R surgery was conducted.

Cell survival assay

Cell survival assay after the challenge of CCl₄, t-BuOOH, RSL3, Cisplatin, ML210 or FINO2 was performed using CellTiter Glo® Luminescent Cell Viability Assay (Promega, MDN, WI, USA). It's a homogeneous method to determine the number of viable cells in culture based on quantitation of the ATP present, which signals the presence of metabolically active cells. A CellTiter Glo Assay (Promega) was performed according to the manufacturer's instructions. Briefly, cells (8000 MEF cells, 10000 Hepa-1c1c7 cells, 8000 Huh7 cells, 6000 primary hepatocytes) were seeded into a 96-well plate (Jet Biofil) and incubated for 24 h at 37 °C with 5% CO₂ prior to subsequent treatment. Indicated doses of chemicals were added into culture medium with 0.1% DMSO. A single reagent (CellTiter Glo® Reagent) was directly added to cells cultured in serum-supplemented medium after chemical challenges for overnight. The luminescence was recorded by the Perkin Elmer plate reader.

Statistical analyses

All assays were conducted at least 3 times and reproducible results were obtained. Results are presented as mean ± Standard Deviation (SD). The statistical significance between different groups was analyzed by paired Student's t test or unpaired two-tailed Student's t test as stated (Prism; GraphPad). Statistical significance was defined as **p* < 0.05; ***p* < 0.01; ****p* < 0.001; *****p* < 0.0001.

DATA AVAILABILITY

Data supporting the present study are available from the corresponding author upon reasonable request.

REFERENCES

- Zhai Y, Busuttill RW, Kupiec-Weglinski JW. Liver ischemia and reperfusion injury: new insights into mechanisms of innate-adaptive immune-mediated tissue inflammation. *Am J Transpl.* 2011;11:1563–9.
- Peralta C, Jimenez-Castro MB, Gracia-Sancho J. Hepatic ischemia and reperfusion injury: effects on the liver sinusoidal milieu. *J Hepatol.* 2013;59:1094–106.
- Guicciardi ME, Malhi H, Mott JL, Gores GJ. Apoptosis and necrosis in the liver. *Compr Physiol.* 2013;3:977–1010.
- Dixon SJ, Lemberg KM, Lamprecht MR, Skouta R, Zaitsev EM, Gleason CE, et al. Ferroptosis: an iron-dependent form of nonapoptotic cell death. *Cell.* 2012;149:1060–72.
- Conrad M, Angeli JP, Vandenabeele P, Stockwell BR. Regulated necrosis: disease relevance and therapeutic opportunities. *Nat Rev Drug Discov.* 2016;15:348–66.
- Jiang X, Stockwell BR & Conrad, M, Ferroptosis: mechanisms, biology and role in disease. *Nat Rev Mol Cell Biol.* 2021;22:266–82.
- Fang X, Wang H, Han D, Xie E, Yang X, Wei J, et al. Ferroptosis as a target for protection against cardiomyopathy. *Proc Natl Acad Sci USA.* 2019;116:2672–80.
- Doll S, Proneth B, Tyurina YY, Panzilius E, Kobayashi S, Ingold I, et al. ACSL4 dictates ferroptosis sensitivity by shaping cellular lipid composition. *Nat Chem Biol.* 2017;13:91–8.
- Stockwell BR, Friedmann Angeli JP, Bayir H, Bush AI, Conrad M, Dixon SJ, et al. Ferroptosis: a regulated cell death nexus linking metabolism, redox biology, and disease. *Cell.* 2017;171:273–85.
- Cheng Y, Zak O, Aisen P, Harrison SC, Walz T. Structure of the human transferrin receptor-transferrin complex. *Cell.* 2004;116:565–76.
- Feng H, Schorpp K, Jin J, Yozwiak CE, Hoffstrom BG, Decker AM, et al. Transferrin receptor is a specific ferroptosis marker. *Cell Rep.* 2020;30:3411–23 e3417.
- Zhong Q, Gao W, Du F, Wang X. Mule/ARF-BP1, a BH3-only E3 ubiquitin ligase, catalyzes the polyubiquitination of Mcl-1 and regulates apoptosis. *Cell.* 2005;121:1085–95.
- Chen D, Kon N, Li M, Zhang W, Qin J, Gu W. ARF-BP1/Mule is a critical mediator of the ARF tumor suppressor. *Cell.* 2005;121:1071–83.
- Adhikary S, Marinoni F, Hock A, Hulleman E, Popov N, Beier R, et al. The ubiquitin ligase HectH9 regulates transcriptional activation by Myc and is essential for tumor cell proliferation. *Cell.* 2005;123:409–421.
- Zhang J, Kan S, Huang B, Hao Z, Mak TW, Zhong Q. Mule determines the apoptotic response to HDAC inhibitors by targeted ubiquitination and destruction of HDAC2. *Genes Dev.* 2011;25:2610–8.
- Wan W, You Z, Zhou L, Xu Y, Peng C, Zhou T, et al. mTORC1-regulated and HUWE1-mediated WIPI2 degradation controls autophagy flux. *Mol Cell.* 2018;72:303–5 e306.
- Hall JR, Kow E, Nevis KR, Lu CK, Luce KS, Zhong Q, et al. Cdc6 stability is regulated by the Huwe1 ubiquitin ligase after DNA damage. *Mol Biol Cell.* 2007;18:3340–50.
- Zhao X, Heng JI, Guardavaccaro D, Jiang R, Pagano M, Guillemot F, et al. The HECT-domain ubiquitin ligase Huwe1 controls neural differentiation and proliferation by destabilizing the N-Myc oncoprotein. *Nat Cell Biol.* 2008;10:643–53.
- Wang L, Luk CT, Schroer SA, Smith AM, Li X, Cai EP, et al. Dichotomous role of pancreatic HUWE1/MULE/ARF-BP1 in modulating beta cell apoptosis in mice under physiological and genotoxic conditions. *Diabetologia.* 2014;57:1889–98.
- Kao SH, Wu HT, Wu KJ. Ubiquitination by HUWE1 in tumorigenesis and beyond. *J Biomed Sci.* 2018;25:67.
- Cheng DD, Yu T, Hu T, Yao M, Fan CY, Yang QC. MiR-542-5p is a negative prognostic factor and promotes osteosarcoma tumorigenesis by targeting HUWE1. *Oncotarget.* 2015;6:42761–72.
- Wang F, Min X, Hu SY, You DL, Jiang TT, Wang L, et al. Hypoxia/reoxygenation-induced upregulation of miRNA-542-5p aggravated cardiomyocyte injury by repressing autophagy. *Hum Cell.* 2021;34:349–59.
- Hao Z, Duncan GS, Su YW, Li WY, Silvester J, Hong C, et al. The E3 ubiquitin ligase Mule acts through the ATM-p53 axis to maintain B lymphocyte homeostasis. *J Exp Med.* 2012;209:173–86.
- Wong FW, Chan WY, Lee SS. Resistance to carbon tetrachloride-induced hepatotoxicity in mice which lack CYP2E1 expression. *Toxicol Appl Pharm.* 1998;153:109–18.
- Kagan VE, Mao G, Qu F, Angeli JP, Doll S, Croix CS, et al. Oxidized arachidonic and adrenic PEs navigate cells to ferroptosis. *Nat Chem Biol.* 2017;13:81–90.
- Yuan H, Li X, Zhang X, Kang R, Tang D. Identification of ACSL4 as a biomarker and contributor of ferroptosis. *Biochem Biophys Res Commun.* 2016;478:1338–43.
- Yang WS, Kim KJ, Gaschler MM, Patel M, Shchepinov MS, Stockwell BR. Peroxidation of polyunsaturated fatty acids by lipoxygenases drives ferroptosis. *Proc Natl Acad Sci USA.* 2016;113:E4966–75.
- Wang H, An P, Xie E, Wu Q, Fang X, Gao H, et al. Characterization of ferroptosis in murine models of hemochromatosis. *Hepatology.* 2017;66:449–65.
- Breitzig M, Bhimineni C, Lockey R, Kolliputi N. 4-Hydroxy-2-nonenal: a critical target in oxidative stress? *Am J Physiol Cell Physiol.* 2016;311:C537–C543.
- Wallach D, Kang TB, Dillon CP, Green DR. Programmed necrosis in inflammation: toward identification of the effector molecules. *Science.* 2016;352:aaf2154.
- Yamada N, Karasawa T, Wakiya T, Sadatomo A, Ito H, Kamata R, et al. Iron overload as a risk factor for hepatic ischemia-reperfusion injury in liver transplantation: potential role of ferroptosis. *Am J Transpl.* 2020;20:1606–18.
- Feng H, Stockwell BR. Unsolved mysteries: How does lipid peroxidation cause ferroptosis? *PLoS Biol.* 2018;16:e2006203.
- Ingold I, Berndt C, Schmitt S, Doll S, Poschmann G, Buday K, et al. Selenium utilization by GPX4 is required to prevent hydroperoxide-induced ferroptosis. *Cell.* 2018;172:409–22 e421.
- Wenz C, Faust D, Linz B, Turmann C, Nikolova T, Bertin J, et al. t-BuOOH induces ferroptosis in human and murine cell lines. *Arch Toxicol.* 2018;92:759–75.
- Friedmann Angeli JP, Schneider M, Proneth B, Tyurina YY, Tyurin VA, Hammond VJ, et al. Inactivation of the ferroptosis regulator Gpx4 triggers acute renal failure in mice. *Nat Cell Biol.* 2014;16:1180–91.
- Thompson JW, Nagel J, Hoving S, Gerrits B, Bauer A, Thomas JR, et al. Quantitative Lys-Gly-Gly (diGly) proteomics coupled with inducible RNAi reveals ubiquitin-mediated proteolysis of DNA damage-inducible transcript 4 (DDIT4) by the E3 ligase HUWE1. *J Biol Chem.* 2014;289:28942–55.
- Fillebeen C, Charlebois E, Wagner J, Katsarou A, Mui J, Vali H, et al. Transferrin receptor 1 controls systemic iron homeostasis by fine-tuning hepcidin expression to hepatocellular iron load. *Blood.* 2019;133:344–55.
- Yang WS, Stockwell BR. Synthetic lethal screening identifies compounds activating iron-dependent, nonapoptotic cell death in oncogenic-RAS-harboring cancer cells. *Chem Biol.* 2008;15:234–45.
- Gammella E, Buratti P, Cairo G, Recalcati S. The transferrin receptor: the cellular iron gate. *Metallomics.* 2017;9:1367–75.
- Zhang MW, Yang G, Zhou YF, Qian C, Mu MD, Ke Y, et al. Regulating ferroportin-1 and transferrin receptor-1 expression: a novel function of hydrogen sulfide. *J Cell Physiol.* 2019;234:3158–69.
- Kawabata H. Transferrin and transferrin receptors update. *Free Radic Biol Med.* 2019;133:46–54.
- Hirayama T, Okuda, K & Nagasawa, H, A highly selective turn-on fluorescent probe for iron(II) to visualize labile iron in living cells. *Chem Sci.* 2013;4:1250–56.
- Gao M, Monian P, Quadri N, Ramasamy R, Jiang X. Glutaminolysis and transferrin regulate ferroptosis. *Mol Cell.* 2015;59:298–308.
- Horonchik L, Wessling-Resnick M. The small-molecule iron transport inhibitor ferristatin/NSC306711 promotes degradation of the transferrin receptor. *Chem Biol.* 2008;15:647–53.
- Dadson K, Hauck L, Hao Z, Grothe D, Rao V, Mak TW, et al. The E3 ligase Mule protects the heart against oxidative stress and mitochondrial dysfunction through Myc-dependent inactivation of Pgc-1alpha and Pink1. *Sci Rep.* 2017;7:41490.
- Jiang L, Kon N, Li T, Wang SJ, Su T, Hibshoosh H, et al. Ferroptosis as a p53-mediated activity during tumour suppression. *Nature.* 2015;520:57–62.
- Tarangelo A, Magtanong L, Biegging-Rolett KT, Li Y, Ye J, Attardi LD, et al. p53 suppresses metabolic stress-induced ferroptosis in cancer cells. *Cell Rep.* 2018;22:569–75.
- Lok CN, Ponka P. Identification of a hypoxia response element in the transferrin receptor gene. *J Biol Chem.* 1999;274:24147–52.
- Tacchini L, Bianchi L, Bernelli-Zazzera A, Cairo G. Transferrin receptor induction by hypoxia. HIF-1-mediated transcriptional activation and cell-specific post-transcriptional regulation. *J Biol Chem.* 1999;274:24142–6.
- Mullner EW, Kuhn LC. A stem-loop in the 3' untranslated region mediates iron-dependent regulation of transferrin receptor mRNA stability in the cytoplasm. *Cell.* 1988;53:815–25.
- Fujita H, Iwabu Y, Tokunaga K, Tanaka Y. Membrane-associated RING-CH (MARCH) 8 mediates the ubiquitination and lysosomal degradation of the transferrin receptor. *J Cell Sci.* 2013;126:2798–809.
- Chen J, Wang J, Meyers KR, Enns CA. Transferrin-directed internalization and cycling of transferrin receptor 2. *Traffic.* 2009;10:1488–1501.
- Sun Q, Fan W, Chen K, Ding X, Chen S, Zhong Q. Identification of Barkor as a mammalian autophagy-specific factor for Beclin 1 and class III phosphatidylinositol 3-kinase. *Proc Natl Acad Sci USA.* 2008;105:19211–6.
- Zhu J, Lu T, Yue S, Shen X, Gao F, Busuttill RW, et al. Rapamycin protection of livers from ischemia and reperfusion injury is dependent on both autophagy induction and mammalian target of rapamycin complex 2-Akt activation. *Transplantation.* 2015;99:48–55.
- Yue S, Zhu J, Zhang M, Li C, Zhou X, Zhou M, et al. The myeloid heat shock transcription factor 1/beta-catenin axis regulates NLR family, pyrin domain-containing 3 inflammasome activation in mouse liver ischemia/reperfusion injury. *Hepatology.* 2016;64:1683–98.

ACKNOWLEDGEMENTS

We appreciate Dr. Tak W Mak (University Health Network, Toronto, Canada) for providing Huwe1-flox mice. We thank Dr. Jixi Li (Fudan University, Shanghai, China), Dr. Xuxu Sun (Shanghai Jiaotong University School of Medicine, Shanghai, China) and Dr. Ming He (Shanghai Jiaotong University School of Medicine, Shanghai, China) for reagents. We thank Academician Prof. Guoqiang Chen (Shanghai Jiaotong University School of Medicine, Shanghai, China) for helpful discussion and suggestions. We also appreciate the support from Shanghai Frontiers Science Center of Cellular Homeostasis and Human diseases, and Core Facility of Basic Medical Sciences, Shanghai Jiao Tong University School of Medicine.

AUTHOR CONTRIBUTIONS

YY, QZ and JZ participated in research design and QX provided the clinical samples to support; YW, HJ, and YY performed cell biology experiments; YW, HJ, YY, YW, and HL did the mice experiment analysis; KH collected the patients samples and HJ did the biochemistry and statistical analysis; YJ and JZ performed the ischemia/reperfusion surgery; ZH made the Huwe1-flox mice strain; HJ and XZ did the primary hepatocytes culture; YY, YW and HJ performed data analysis and interpretation; YW and HJ drafted the paper; HJ did the graphical abstract. JZ supervised the study and contributed to the writing of the manuscript. and All authors read and approved the final manuscript.

FUNDING

This work was supported by National Natural Science Foundation of China (32070734), Natural Science Foundation of Shanghai (20ZR1430800), the Shanghai Pujiang Program (20PJ1409500) to JZ, National Natural Science Foundation of China (91754205, 91957204, 31771523), Ministry of Science and Technology of China (2019YFA0508602), the Sino-German Mobility Program (M-0140), Program of Shanghai Subject Chief Scientist (19XD1402200) to QZ, Project of Shanghai key clinical specialties (shslczdzk05801) and Innovative Research Team of High-Level Local Universities in Shanghai (SSMU-ZDCX20180802) to QX, Medical-Engineering

Cross-Research Fund in "Jiaotong University Star" Program of Shanghai Jiao Tong University (YG2022QN002) to HJ, Project of the Shanghai Municipal Health Commission (20204Y0012) to KH, innovative research team of high-level local universities in Shanghai and Shanghai Science and Technology Commission (20JC1410100).

ETHICAL STATEMENT

All animal experiments were conducted in agreement with the Guide for the Care and Use of Laboratory Animals and approved by the Institutional Animal Care and Use Committee of Shanghai Jiao Tong University School of Medicine (Shanghai, China). This study related to patients has been approved by the Institutional Review Board of Renji Hospital affiliated to Shanghai Jiao Tong University School of Medicine (IRB Reference Number: KY2020-190). The participants or their guardians provided signed consent.

COMPETING INTERESTS

The authors declare no competing interests.

ADDITIONAL INFORMATION

Supplementary information The online version contains supplementary material available at <https://doi.org/10.1038/s41418-022-00957-6>.

Correspondence and requests for materials should be addressed to Yangbo Yue, Qiang Xia, Qing Zhong or Jing Zhang.

Reprints and permission information is available at <http://www.nature.com/reprints>

Publisher's note Springer Nature remains neutral with regard to jurisdictional claims in published maps and institutional affiliations.